Article

Novel Flavanone Naringenin Derivative with Anti-Inflammatory Activity

Rodrigo O. S. de Souza,[a] Lívia C. R. Hilgenberg,[a] Ana C. S. Pinto,[a] Renyer A. Costa,[b]
Fernanda G. Simplicio [a] and Emerson S. Lima [,a]*

[a]*Faculdade de Ciências Farmacêuticas, Universidade Federal do Amazonas, 69077-000 Manaus-AM, Brazil*

[b]*Departamento de Química, Instituto de Ciências Exatas, Universidade Federal do Amazonas,*
69077-000 Manaus-AM, Brazil

Naringenin is a flavonoid with several biological activities already reported but with few biological applications in the pharmaceutical field. In this work, a new flavanone, called carboxymidamide (DCHA), synthesized through the condensation reaction between naringenin and aminoguanidine is structurally confirmed through spectroscopic analysis of nuclear magnetic resonance, mass spectrometry and Fourier transform infrared. DCHA was not toxic to human fibroblasts and inhibited macrophage activation *in vitro*. *In vivo*, it suppressed leukocyte migration in lipopolysaccharide (LPS)-induced peritonitis and reduced zymosan-induced paw edema. Molecular docking simulations of DCHA in the active site of the enzymes inducible nitric oxide synthase, cyclooxygenase-2 and phosphodiesterase type 4 indicate that the anti-inflammatory activity of this new flavanone can be explained by the inhibition of these target enzymes. This is the first work to present the synthesis of a flavonoid derivative with aminoguanidine that showed a high anti-inflammatory potential.

Keywords: carboximidamide, aminoguanidine, naringenin, condensation reaction, macrophages, anti-inflammatory

Introduction

Inflammation is a physiological and protective reaction of the human body that results in the activation of the immune system and is mediated mainly by macrophages.[1] The inflammatory process in disequilibrium with the accentuated release of inflammatory mediators is strongly associated with the emergence of several chronic diseases, such as arthritis, diabetes and cancer.[2,3] Therefore, the discovery of new therapeutic agents with anti-inflammatory action is still necessary.[3] In this context, natural products are the main source of new drugs, especially anti-inflammatory drugs, resulting from structural changes.[4-6] Flavonoids are the most studied phytochemical classes of natural products due to their wide spectrum of pharmacological properties and their various modifications from their base structures (C6-C3-C6), with the aim of increasing or potentiating their pharmacotherapeutic actions.[7,8]

Naringenin (NAR) is a flavonoid that belongs to the flavanone class and is present in citrus fruits and tomatoes. NAR is a naringin aglycone that has an excellent anti-inflammatory effect but has low solubility. Among the biological activities described for this flavanone are anticancer, antiatherogenic, anti-inflammatory, antioxidant, prevention of atherosclerosis, among others.[8-10] A recent study[11] observed that NAR exerts anti-inflammatory action by inhibiting the nuclear factor kappa B (NF-kB) signaling pathway, which is associated with stimulating the expression of several important inflammatory proteins, such as tumor necrosis factor alpha (TNF-α), interleuin-6 (IL-6), interleukin-1 (IL-1), cyclooxygenase-2 (COX-2) and inducible nitric oxide synthase (iNOS).[11] Fan *et al.*[12] demonstrated that this flavanone exerts a potent anti-inflammatory effect, significantly decreasing TNF-α levels, in addition, reduced NF-kB messenger ribonucleic acid (mRNA) levels in an experimental model of arthritis.

Zhang *et al.*[13] synthesized three new narigenin derivatives from the biotransformation of narigenin by *Bacillus amyloliquefaciens*, naringenin 7-*O*-phosphate, naringenin 7-*O*-glucoside (prunin), and 6''-*O*-succinylprunin, where the study also revealed that the derivative naringenin 7-*O*-phosphate has approximately 45-fold higher water solubility than that of naringenin, resulting in improved antibacterial activity. Copmans *et al.*[14]

*e-mail: eslima@ufam.edu.br
Editor handled this article: Brenno A. D. Neto

studied naringenin derivatives obtained through the methylation of free hydroxyl groups, demonstrating efficacy against seizures.

Aminoguanidine (AG) is a drug that was synthesized over 100 years ago through the reduction of nitroguanidine, which inhibits the formation of advanced glycosylation end products (AGEs), being used for the treatment of diabetes, furthermore inhibits iNOS. The effect of AG on the inhibition of iNOS induced on the degree of healing of periapical lesions was evaluated, demonstrating an anti-inflammatory effect on the healing of these lesions.[15,16] Misko *et al.*[17] demonstrated that aminoguanidine selectively inhibited iNOS expressed by macrophages activated by lipopolysaccharide (LPS) during the inflammatory process. Despite its effectiveness, the substance has toxic side effects that make its pharmacological use unfeasible.[15]

In the present study, the semisynthesis of the flavanone carboximidamide (DCHA) molecule was performed by condensation of NAR with AG, with the aim of obtaining an unprecedented substance with potentiated anti-inflammatory activity and without toxic effects. Its anti-inflammatory potential was evaluated via its ability to inhibit NO• release in J774A.1 macrophages stimulated by LPS *in vitro*, as well as in LPS-induced peritonitis and zymosan-induced paw edema in mice. Cytotoxicity was assessed by using the Alamar Blue method. Guided by the *in vitro* and *in vivo* results, and aiming to justify the experimental anti-inflammatory properties of DCHA, molecular docking calculations were performed with the enzymes iNOS, COX-2 and phosphodiesterase type 4 (PDE4) to evaluate binding energies and interactions involved in binding sites, since PDE4 inhibitors are known to have beneficial effects in metabolic diseases, in inflammatory and cognitive disorders.[18] COX-2 inhibitors are effective NSAIDs (non-steroidal anti-inflammatory drugs) and iNOS overexpression increases NO• levels, which are associated with complex multifactorial diseases such as Parkinson's disease, Alzheimer's disease, multiple sclerosis, rheumatoid arthritis and inflammatory bowel disease.[19]

Experimental

Materials and methods

Reagents

The (±) naringenin (NAR) and aminoguanidine (AG) used in the synthesis of the derivative were purchased from Sigma-Aldrich (St. Louis, USA), as were the other reagents used in the biological assays. Cell lines of human fibroblasts (MRC-5) and murine macrophages J774A.1 were acquired from the cell bank of the Faculty of Pharmaceutical Sciences (FCF) of the Universidade

Federal do Amazonas (UFAM) (Manaus, Brazil). Roswell Park Memorial Institute (RPMI) 1640 culture medium and penicillin-streptomycin were purchased from Gibco (Grand Island, USA) and fetal bovine serum (FBS) from Gibco (Paisley, UK).

Synthetic materials and methods

All the solvents and reagents were obtained from commercial suppliers. Silica gel 60, 230-400 mesh, 40-63 μm, for column chromatography and thin layer chromatography (TLC) silica gel 60 F_{254} plates were obtained from Merck (Darmstadt, Germany). Nuclear magnetic resonance (NMR) spectra were recovered on a Bruker Ascend 500 MHz Biospin instrument 7.0 Tesla Fourier model 300 (Bremen, Germany) using deuterated dimethylsulfoxide (DMSO, $(CD_3)_2SO$) as solvent and chemical shifts are reported in parts *per* million (ppm) in relation to tetramethylsilane (TMS) as the internal standard both from Sigma-Aldrich (St. Louis, MO, USA). The chemical shifts (δ) are in ppm and J values in hertz (Hz). Mass spectra were measured on an ion-trap spectrometer (LCQ Fleet, Thermo Scientific) operating with an electron spray source (ESI) in the positive mode (ESI-MS/MS-MS). The infrared spectra were recorded using KBr pellets (for solid) in the Fourier transform infrared (FTIR) spectrophotometer (Shimadzu IR Prestige-21) and the values are reported in ν wave numbers (400-4000 cm^{-1}) and with a spectral resolution of 4 cm^{-1}.

General procedure for the preparation of the flavanone carboximidamide (DCHA)

In a 50 mL flask containing NAR (50.8 mg, 0.19 mmol) (Sigma-Aldrich, USA), AG (55.5 mg, 0.47 mmol) (Sigma-Aldrich, USA) and 10 mL of ethanol, concentrated HCl (1 mL) and distilled water (1 mL) were added.[20] This was stirred and heated (70 °C) for 6 h. Product formation was monitored using TLC, then eluted with AcOEt:acetone:H_2CO_2 (4:1:0.5). The residue obtained was washed with distilled water (20 mL), NaHCO$_3$ (aqueous) and extracted with ethyl acetate. The dry residue was redissolved in ethanol (10 mL) with 1 M HCl (10 mL) added and stirred for 1 h. The mixture was evaporated and the residue was recrystallized from ethanol to precipitate the product.

(2E)-2-[5,7-Dihydroxy-2-(4-hydroxyphenyl)-2,3-dihydro-4H-1-benzopyran-4-ylidene]hydrazine-1-carboximidamide (DCHA)

Brown solid; yield: 81%; IR (KBr) ν / cm^{-1} 3500-3000, 1630-1450, 1600-1800, 1490, 1250-1080, 1150; ^{1}H NMR

(500 MHz, $(CD_3)_2SO$) δ 2.93 (dd, 1H, *J* 12.2, 16.8 Hz, CH), 3.19 (dd, 1H, *J* 3.1, 16.8 Hz, CH), 5.10 (dd, 1H, *J* 2.7, 12.2 Hz, CH), 5.92 (d, 1H, *J* 2.4 Hz, CH), 5.95 (d, 1H, *J* 2.4 Hz CH), 6.81 (m, 2H, CH), 7.30-7,84 (m, 2H, CH), 8.65 (s, $-NH_2$), 9.60 (s, 1H, C4'-OH), 9.75 (s, 1H, =NH), 10.76 (s, 1H, C7-OH), 10.86 (s, 2H, -NH-), 12.13 (s, 1H, C5-OH); ^{13}C NMR (125 MHz, $(CD_3)_2SO$) δ 24.45, 68.25, 87.29, 88.47, 89.73, 102.70, 106.87, 119.39, 120.22, 121.75, 147.72, 149.51, 150.53, 151.53, 152.47, 154.79; HRMS (ESI/MS) *m/z*, calcd. for $C_{16}H_{16}N_4O_4$ [M]$^+$: 328.32, found [M + H]$^+$: 329.

Molecular docking simulations

Molecular docking calculations were performed with the help of AutoDock Vina software with COX-2, iNOS and PDE4a achieved from Protein Data Bank (PDB) under codes 4COX, 1QW5 and 3I8V respectively.[21-23] The docking protocol consisted in removal of water molecules as well as ligands, Gasteiger charges were assigned and the macromolecule was saved in PDBQT file format using ADT (autodock tools) software. The docking protocol consisted in removing water molecules and inhibitors, assigning Gasteiger charges and delimiting a grid box with dimensions 18 Å ×18 Å × 18 Å for COX-2, 20 Å × 18 Å × 18 Å for iNOS and 22 Å × 20 Å × 20 Å for PDE4a, centered in the active site of each enzyme, with coordinates X = 25.537, Y = 22.738, Z = 14.629 (COX-2), X = −53.145, Y = 135.190, Z = 44.905 (iNOS) and X = 43.365, Y = 17.859, Z = −24.518 (PDE4a). The docking protocol was tested by removing the co-crystallized inhibitors from the target proteins and then docking them at the active site. The superimposition of the inhibitors (docked and co-crystalized) showed root-mean-square deviation (RMSD) values of 1.2020, 2.7200 and 1.203 Å for indomethacin (inhibitor of COX-2), *N*-(3-(aminomethyl)benzyl)acetamidine (inhibitor of iNOS), and for 4-(3-butoxy-4-methoxyphenyl)methyl-2-imidazolidone (inhibitor of PDE4a), respectively. DCHA structures (*R* and *S* enantiomers) used in the docking calculations were modeled via density functional theory (DFT), using B3LYP (Becke, 3-parameter, Lee-Yang-Parr) exchange-correlation functional and 6-31G(d) basis set with the help of Gaussian 09 program.[24]

Cytotoxicity test

The cytotoxicity of the substances (DCHA, NAR and AG) in the culture of the human lung fibroblast cell line MRC-5 was determined using the Alamar Blue method, which is known as resazurin (Sigma-Aldrich, USA) in its non-fluorescent oxidized state, and a dose-response curve was constructed. In viable cells, enzymes present within the mitochondria reduce resazurin to pink fluorescent resofurin.[25] MRC-5 cells were incubated (37 °C, 5% CO_2) and supplemented with fetal bovine serum (10%), penicillin (50 U mL^{-1}) and streptomycin (50.0 µg mL^{-1}). Then, cells were seeded at a density of 5×10^3 cells well^{-1} in 96-well plates. After 24 h of incubation and cell adhesion, they were treated with the substances mentioned above, at concentrations of 12.5, 50, 200 and 800 µg mL^{-1}, using doxorubicin (10 µg mL^{-1}) as a positive control for toxicity and, as a negative control, the culture medium and DMSO (0.1% v/v). After the 24 h treatment period, 10 µL of 0.4% resazurin (diluted 1:20) were added, and 3 h later (resazurin metabolization period) the resulting fluorescence reading was performed in a spectrophotometer, with excitation at 570 nm and emission at 610 nm. The percentage of viable cells was calculated based on the negative control.[26]

Inhibition of macrophage activation by LPS

In order to evaluate the production of nitric oxide (NO$^\bullet$) by LPS-stimulated J774A.1 macrophages, the levels of nitrite in the culture medium were determined using the Griess reaction. J774A.1 murine macrophage cells were seeded at a concentration of 1×10^6 cells well^{-1} in a 96-well plate. After incubating the cells at 37 °C in a 5% CO_2 atmosphere for 24 h, the RPMI medium was supplemented with 1% FBS with a final volume of 100 µL well^{-1}. Then, the cells were stimulated with 1 µg mL^{-1} of LPS extracted from *Escherichia coli* serotype 450111:B4 (Sigma-Aldrich, Germany) and treated with the substances (DCHA, NAR and AG) at concentrations of 2.5, 5, 10 and 20 µg mL^{-1}. As the positive control, RPMI 1640 medium enriched with LPS was used and, as the negative control, RPMI 1640 medium without LPS. Cell supernatant was collected for nitric oxide (NO$^\bullet$) analysis.

In vivo assays

Animals

Male Swiss Webster mice (*Mus musculus*), 6 weeks old and weighing between 28-32 g, were acquired from the Central Animal House of the Federal University of Amazonas (UFAM), then housed in standard cages in temperature-controlled rooms at 22 ± 2.0 °C, with a 12 h light/dark cycle and access to food and water *ad libitum*. All animal protocols were approved by the Ethics Committee on the Use of Animals (CEUA) of the

J. Braz. Chem. Soc. **2024**, *35*, 4, e-20230157

3 of 12

Federal University of Amazonas (UFAM), via process No. 026/2019.

LPS-induced peritonitis

Acute inflammation was induced with bacterial LPS intraperitoneally (IP) in the mice, according to the methodology of Marques *et al.*[27] with modifications. Initially, the mice were divided into 6 groups (4 animals *per* group). The animals were orally pre-treated with dexamethasone, DCHA, naringenin and aminoguanidine at a dose of 1 mg kg^{-1} and, after one hour of treatment, peritonitis was induced by a single injection (IP) of LPS (0.2 mL of LPS 500 ng *per* cavity) in the test groups. In the control groups, animals received the vehicle (0.9% saline, 10 mL kg^{-1}) orally and injections (IP) of saline or LPS. After four hours, the animals were euthanized with ketamine:xylazine (180 mg kg^{-1}:30 mg kg^{-1}, IP).

After this procedure, the peritoneal cavity was washed with 10 mL of ice-cold phosphate-buffered saline (10 mM, pH 7.4) containing 3 mM ethylenediaminetetraacetic acid. The cavity was gently massaged three times and the cell suspension was aspirated with a 5 mL syringe. Aliquots of the abdominal fluid were placed in Eppendorf tubes and successively stained with Turk's solution so the total leukocytes could be counted in a Newbauer chamber.

Zymosan-induced paw edema

This assay was performed according to the methodology established by Felix *et al.*[28] with modifications. The mice were divided into five groups (4 animals/group) and treated with the substances DCHA, NAR and AG at a dose of 5 mg kg^{-1}, diclofenac at a dose of 100 mg kg^{-1} as standard control, and saline as a negative control. After one hour, a subplantar injection with 10 μL of the Zimosan solution (100 μg/10 μL saline) was administered to the right hind paw of the mice. The degree of edema in the paws of the animals was measured with a digital caliper immediately before (time 0) and 1 and 6 h after the zymosan injection. At the end of the experiment, the percentage of edema in relation to the control paw of the animals was calculated.

Statistical analysis

The results were expressed as mean ± DPM (standard deviation of the mean) and the means were analyzed using the GraphPad Prism® 6.0 software,[29] using one-way ANOVA analysis of variance, followed by Tukey's or Dunnett's tests of multiple comparisons with a significance level of $p < 0.05$.

Results and Discussion

Synthesis of DCHA

The condensation reaction between NAR and AG, followed by dehydration, gave rise to a brown-colored crystalline molecule characterized as (2*E*)-2-[5,7-dihydroxy-2-(4-hydroxyphenyl)-2,3-dihydro-4*H*-1-benzopyran-4-ylidene]hydrazine-1-carboximidamide (DCHA) with a post-reaction yield of approximately 81% (Figure 1). The reaction between AG and ketone groups contributes to a synthetic route for obtaining carboximidamide derivatives.[30,31] The double bond between carbon and nitrogen plays an important role in the bioactivity of carboximidamide derivatives, which has been emphasized in previous studies[31] of structure-activity relationship in synthetic models for obtaining new derivatives with specific biological activities. Wei *et al.*[32] synthesized chalcone derivatives with AG, which are called acylhydrazones. These derivatives proved to be effective anti-inflammatory drugs, with a response of 92.45%, while the reference drugs used, ibuprofen and indomethacin, had an efficiency of 87.36 and 89.36%, respectively. The addition of AG to the structures of the chalcones accentuated the anti-inflammatory *in vitro* activity of these molecules.
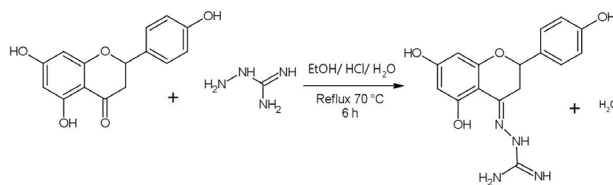

Figure 1. Condensation reaction between naringenin (NAR) and aminoguanidine (AG) in alcoholic acid, giving rise to the DCHA derivative.

Chemical characterization of DCHA

After chemical determination and characterization, the substance DCHA was identified as a flavanone carboximidamide. The carboximidamide is a chemical class with multiple pharmacological properties that have potential for application in the treatment of chronic diseases of metabolic and inflammatory origin.[31] The reaction between the carbonyl of the C ring of the NAR with the amine of the AG resulted in the formation of a hydrazine, also known as Schiff's base, which is a functional group with anti-glycation, antioxidant and anti-inflammatory properties.[33] The estimated molecular mass of the DCHA derivative was 328 g mol^{-1}. The mass spectrometry analysis showed a base peak of [M + H]$^+$ 329 g mol^{-1}, confirming the presence of the expected product, since in the positive mode

there is an addition of a proton in the analyzed structure (Figure S1, Supplementary Information (SI) section). The fragmentation spectrum (MS/MS) of the ion at *m/z* 329 (Figure S2, SI section) revealed the presence of the mass/charge fragments with *m/z* 312 and 270, resulting from the losses of the amine and guanidine groups of the AG, and showed the occurrence of the reaction between NAR and AG. The *m/z* 209 fragment characterizes the loss of the 4-ethylphenol group of the flavonoid. The presence of the *m/z* 203 fragment refers to the loss of the –C_3O_2 group of NAR.[34,35] Ye *et al.*[36] observed similar fragmentation in the characterization of *Millettia nitida* flavonoids, whose spectrum corresponded to flavanones and a catechin.[37] The ^{1}H and ^{13}C NMR spectra (Figures S3 and S4, SI section) of the DCHA derivative showed a profile that is similar to the shifts found for NAR and AG, which show the signals attributed to the aromatic ring carbons A and B of the NAR, with shifts at *δ* 87.29 and 88.47 ppm for methine carbons, of ring A and for methine carbons at *δ* 120.22, 119.39 and 106.87 ppm for carbons C-2', C-3', C-5 'and C-6' of ring B. Furthermore, a signal was observed at *δ* 154.79 ppm for guanidyl, confirming the addition of the AG group in the molecule, replacing the oxygen on the C-4 carbon. The absence of the peak at *δ* 195 in the ^{13}C NMR spectrum was also observed. By comparing these signals with the distortionless enhancement by polarization transfer 135 (DEPT-135) spectrum (Figure S5, SI section), it was possible to confirm the multiplicity of carbons in the chain.[20,38,39] Infrared (IR, Figure S6, SI section) spectroscopy identified the functional groups that make up the molecule, and the absorption regions shown in the spectrum were similar to those described in the literature for flavonoids. These bands refer to the stretching of C=O (1600-1800 cm^{-1}), stretching of C–O (1080-1250 cm^{-1}), stretching of OH (3100-3290 cm^{-1}), stretching of the C–C connection (1150 cm^{-1}) and the stretching of C=C (1450-1630 cm^{-1}). However, the molecule showed strong peaks in the region of 3000 to 3500 cm^{-1}, corresponding to the stretching vibration that occurs in the O–H and N–H corresponding to the stretching vibration that occurs in the O–H and N–H connections, with a peak at 1490 cm^{-1}, which belongs to the N–H flexion vibration[38,39] (Figure S6).[39,40] Data from the ^{1}H and ^{13}C NMR spectra were compared with data from the literature[41,42] and corroborate with the data presented in our spectra for NAR and AG.

Molecular docking

Molecular docking is a very efficient tool used to simulate the interaction between a small molecule and a protein, making the evaluation of the interaction of such molecules at the binding site of the target proteins possible, and allowing the elucidation of fundamental biochemical processes.[42] AutoDock-Vina, a software used in docking simulations, uses a scoring function consisted in a number of sequential steps on random perturbation of the conformation followed by a local optimization using the Broyden-Fletcher-Goldfarb-Shanno algorithm, being useful to simulate the non-covalent binding of a small molecule (ligand) and a protein (receptor) efficiently.[21] Due to the fact that a chiral mixture of NAR was used for the synthesis of DCHA, the structures of the (*S*)-DCHA and (*R*)-DCHA enantiomers were optimized via DFT using B3LYP/6-31(d) level of theory (Figure 2), which were converted to pdbqt format and used in docking calculations. In relation to binding energies, for the higher score conformations, (*S*)-DCHA showed values −9.8, −10.4 and −9.4 kcal mol^{-1} at COX-2, iNOS and PDE4 active sites respectively, (*R*)-DCHA showed values −7.8, −9.2 and −8.4 kcal mol^{-1} at the active sites of the enzymes, while the inhibitors showed values −10.3 (indomethacin), −6.7 (*N*-(3-(aminomethyl) benzyl)acetamidine) and −7.4 kcal mol^{-1} (4-(3-butoxy-4-methoxyphenyl)methyl-2-imidazolidone). The binding energies indicate that the anti-inflammatory activity of this new flavanone could be explained by the inhibition of COX-2, iNOS and PDE4a enzymes, with emphasis on the inhibition of iNOS and PDE4, where both DCHA enantiomers showed higher docking energies compared to the inhibitors. Figures 3 and 4 show the docking interactions obtained for (*S*)-DCHA and (*R*)-DCHA, respectively, at the active sites of the selected enzymes.
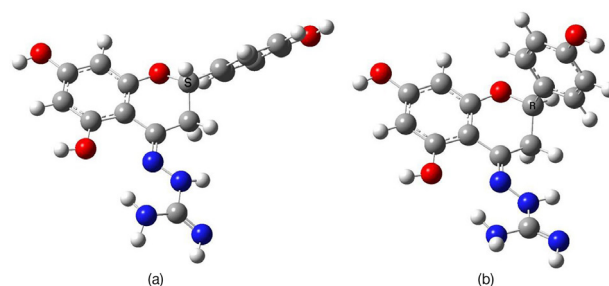

Figure 2. Optimized structures of (*S*)-DCHA (a) and (*R*)-DCHA (b) calculated via DFT at B3LYP/6-31G(d).

Regarding COX-2, binding modes analysis show that (*S*)-DCHA (Figures 3a and 3b) docked at the active site of the enzyme through the formation of ten hydrogen bonds (where seven H-bonds involve the aminoguanidine moiety) with Leu 352, His 90, Ser 353, Tyr 355, Val 349, Ala 527, Trp 387, Glu 192; pi-sigma interaction with Ala 527; pi-alkyl and alkyl-alkyl interactions with Phe 518, Val 523 and Leu 352; carbon hydrogen bond with Val 523. For (*R*)-DCHA (Figures 4a and 4b), binding analysis show

J. Braz. Chem. Soc. **2024**, *35*, 4, e-20230157

5 of 12

at the binding site of COX-2, eight hydrogen bonds (four H-bonds involving the aminoguanidine moiety) with His 90, Gln 192, Phe 518, Tyr 355, Arg 120, Val 523 and Gly 526, pi-sigma interaction with Ala 527, pi-alkyl and alkyl interactions with Val 349 and Leu 352. Indomethacin, show, in the binding pocket, interactions with Ala 527, Val 349, Leu 531, Val 523, Ser 353, Trp 387, His 90, Leu 384, Tyr 355 and Arg 120. The comparison of the binding pocket interactions reveals that (*S*)-DCHA and (*R*)-DCHA show interactions close to those of indomethacin; however, more hydrogen bonds occur for the DCHA enantiomeres, actually, great part promoted by the aminoguanidine moiety. Comparing the two enantiomers of DCHA, it is possible to infer that the *S* enantiomer interacts better with the active site of COX-2, since it forms more hydrogen

interactions, in addition to more interactions between the hydrophobic portion of the site and the phenolic ring of the *S* enantiomer.

For iNOS, binding modes analysis revealed that (*S*)-DCHA (Figures 3c and 3d) docked at the active site by ten hydrogen bonds with Gly 365, Trp 366, Asn 348, Gln 257, Arg 260, Aps 274 and Tyr 341 and two H-bonds with heme (great part of these interactions involve narigenin moiety). In addition, in the pocket site, pi-cation and charge interactions with Aps 376, Glu 371 and heme, pi-alkyl interaction with Val 346 and pi-sigma interaction with Pro 344 were observed. (*R*)-DCHA (Figures 4c and 4d) showed less interactions at the iNOS active site compared to the *S* enantiomer, being noteworthy five hydrogen bonds with Aps 376, Glu 371 and heme, pi-cation and
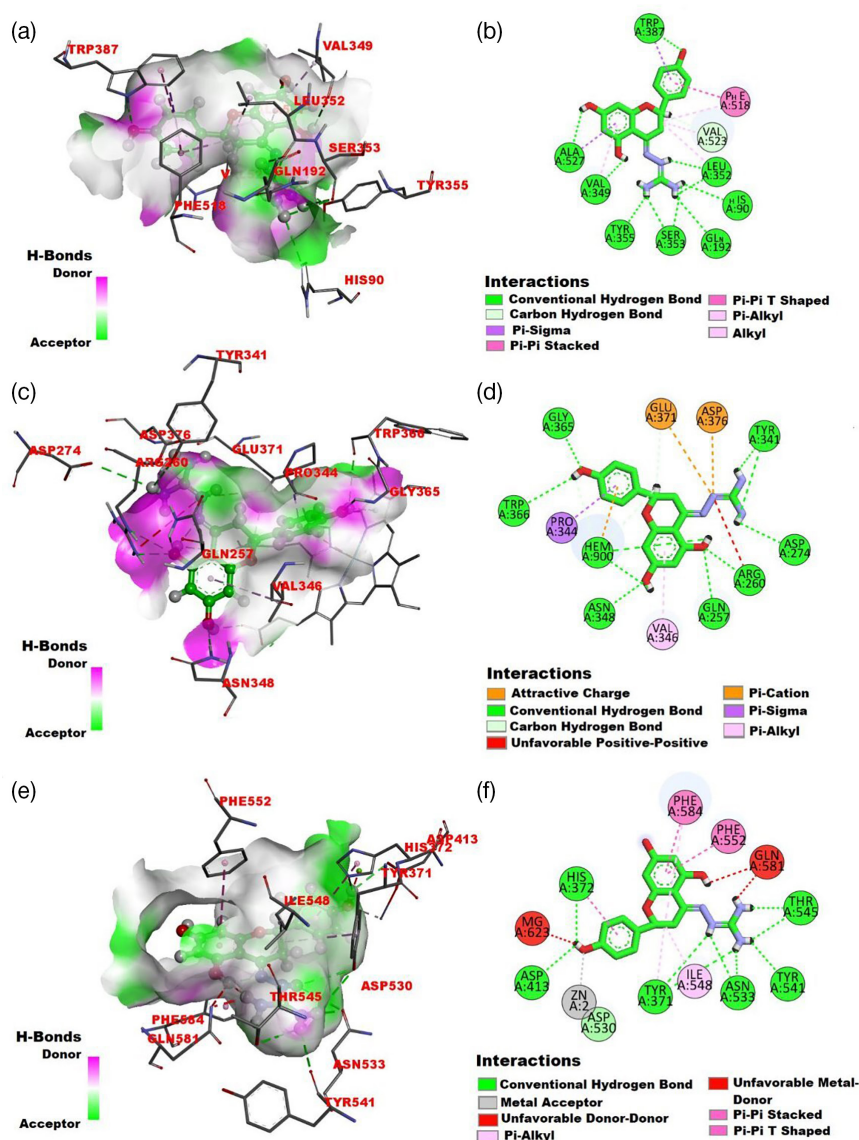

Figure 3. Docking interactions of (*S*)-DCHA at the binding pocket of target enzymes: COX-2-3D representation with H-bond active surface (a); COX-2-2D representation (b); iNOS-3D representation with H-bond active surface (c); iNOS- 2D representation (d); PDE4a-3D representation with H-bond active surface (e); PDE4a-2D representation (f).
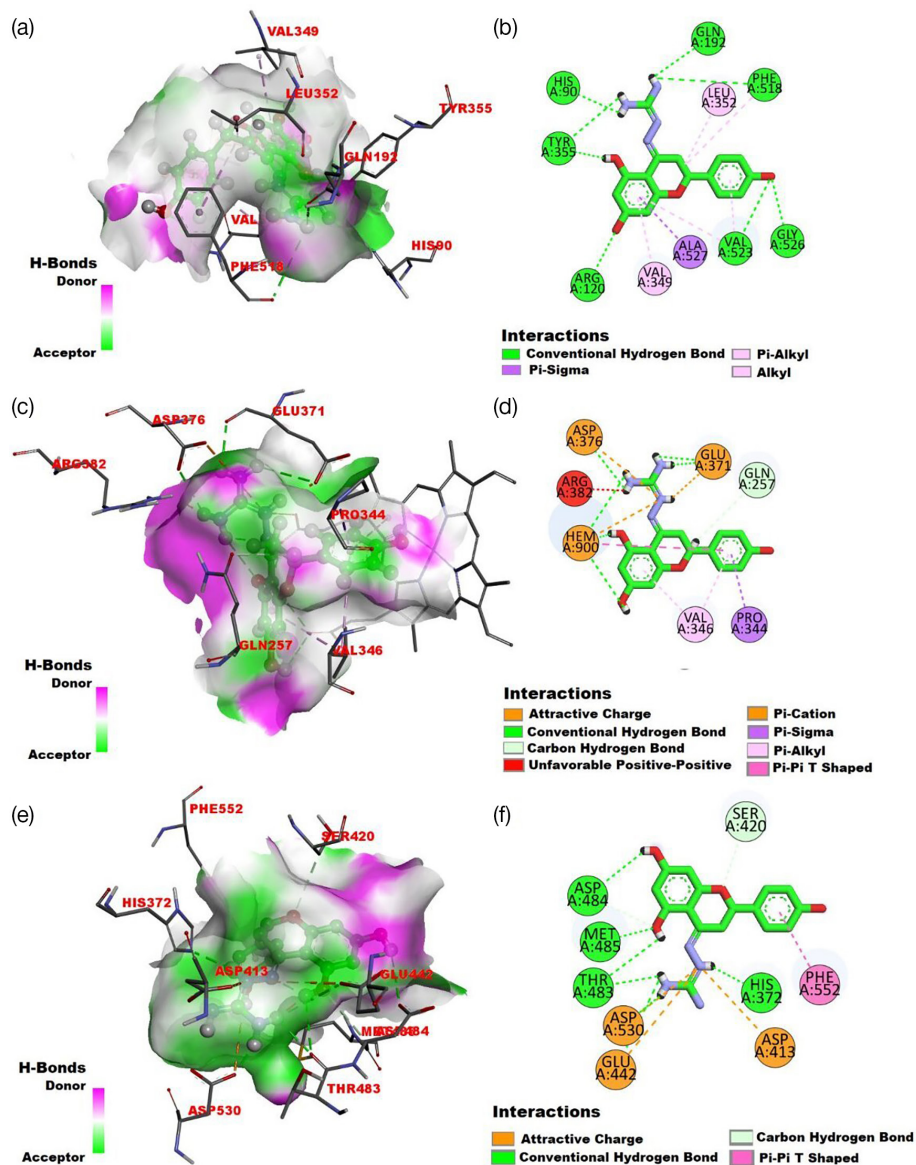
Figure 4. Docking interactions of (*R*)-DCHA at the binding pocket of target enzymes: COX-2-3D representation with H-bond active surface (a); COX-2-2D representation (b); iNOS-3D representation with H-bond active surface (c); iNOS- 2D representation (d); PDE4a-3D representation with H-bond active surface (e); PDE4a-2D representation (f).

charge interactions with Asp 376, Glu 371 and heme, pi-sigma with Pro 344, pi-alkyl with Val 346, pi-pi with heme and carbon. The *S* configuration of carbon 2 of the naringenin moiety provides the enantiomer with a more effective interaction of the aminoguanidine moiety with the hydrophilic moiety of the active site of the iNOS enzyme, evidencing a more efficient interaction of the (*S*)-DCHA molecule, which justifies the higher energy of binding of the *S* enantiomer (–10.4 kcal mol⁻¹), compared to the *R* enantiomer (–9.2 kcal mol⁻¹).

Concerning phosphodiestarese 4a (PDE4a), (*S*)-DCHA (Figures 3e and 3f) complexed with the enzyme through the formation of nine H-bonds in the binding pocket (in which seven involved the aminoguanidine moiety) with

Thr 545, Tyr 541, Asn 533, Tyr 371, Asp 413 and His 372 followed by three pi-pi interactions with Phe 584, Phe 552 and His 372, metal-acceptor type interaction with Zn, pi-pi interactions with Phe 584 and Phe 552. (*R*)-DCHA docked at the PDE4a active site by six H-bonds with Asp 484, Met 485, Thr 483, Glu 442 and His 372, charge interactions with Aps 530, Glu 442 and Aps 413, carbon hydrogen bond with Ser 420 and pi-pi interaction with Phe 552. Similar to the previous interactions, the *S* enantiomer presented a better interaction with the active site of the PDE4a enzyme. In this case, the *S* configuration allows a better interaction of the phenol group with Zn and with the donor H-bond region comprising amino acids His 372 and Aps 413. In fact, molecular docking simulations show

that (*S*)-DCHA and (*R*)-DCHA are possibly a promising inhibitor of COX-2, iNOS and PDE4a enzymes, indicated by the large number of interactions formed in the active sites of these enzymes (mainly H -bond), with emphasis on the *S* enantiomer, which bound more efficiently to enzymes active sites compared to the *R* enantiomer, being noteworthy the interaction with COX-2 enzyme.

Cytotoxicity

In MRC-5 fibroblasts, DCHA and AG did not present cytotoxicity at the concentrations tested, with viability greater than 80% at all concentrations. NAR showed cytotoxicity only at the concentration of 800 µg mL^{-1} (Figure 5). The results showed that the tested substances are considered safe *in vitro* and unlikely to be toxic in *in vivo* tests. When the percentage of viable cells is above 80%, it is not considered cytotoxicity, when this percentage is between 80 and 60%, it is classified as low cytotoxicity.[43] DCHA showed a small reduction in cell viability only at high concentrations *in vitro*. NAR showed low cellular toxicity at a concentration of 200 µg mL^{-1}. Despite this, NAR has a known cytotoxic activity, mainly against cancer cells (SNU-213) whose flavanone apoptotically promotes the death of these cells. However, this effect occurs in concentrations close to 200 to 600 µM.[44] High cytotoxic activity of NAR, as well as its prenylnaringenin derivative, was observed in cancer cells of the U-118 MG lineage and in normal human fibroblasts at concentrations greater than 150 µM.[45] It was observed that AG tends to inhibit cell death due to its antioxidant effect, damage reduction of reactive oxygen species and inhibition of iNOS action.[46]
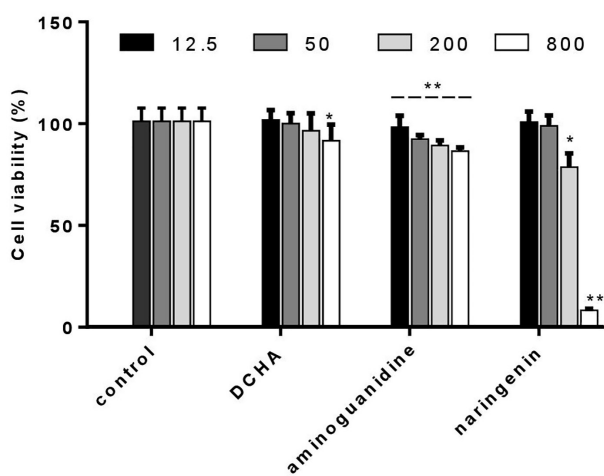

Figure 5. Cell viability in MRC-5 fibroblasts. DCHA, AG and NAR were tested in THP-1 cells for 48 h and MRC-5 for 24 h. Data expressed as mean ± standard deviation, analyzed by two-way ANOVA followed by Dunnett's test (n = 4, *p < 0.05; **p < 0.01).

LPS macrophage activation assay

J774A.1 macrophage cells were activated with 1 µg mL^{-1} of LPS in order to evaluate the ability of DCHA, NAR and AG to inhibit the production of nitric oxide in these cells. The concentrations used ranged from 0.625 to 20 µmol L^{-1}. All the tested substances were able to inhibit the nitric oxide release in the activated macrophages. However, DCHA and AG demonstrated a more significant reduction in the concentration of cellular nitric oxide (Figure 6). It was observed that there was no significant variation in between tested doses of NAR. In a comparison between the effects presented at the tested doses of DCHA (inhibitory concentration (IC$_{50}$) 0.70 µmol L^{-1}) and AG (IC$_{50}$ 2.70 µmol L^{-1}), it was observed that the former demonstrated more significant inhibitory potential (< 0.0001) compared to the second, with DCHA maintaining NO$^{\bullet}$ production below 50 µmol L^{-1}. These results corroborate with the literature,[47] in which NAR significantly reduced the production of NO$^{\bullet}$ in RAW 274.6 cells stimulated by LPS, in addition to the significant suppression of iNOS in these cells. The LPS-stimulated cell expresses iNOS, thereby resulting in the production of NO•. Due to the importance of iNOS, the search for new inhibitors of this isoform is one of the most promising perspectives for the treatment of inflammatory processes. For this purpose, this method of measuring iNOS activity is used, in which the macrophage cell line is stimulated by LPS to express iNOS, and then the production of NO$^{\bullet}$ is detected through the addition of Griess' reagent.[48]

LPS-induced peritonitis

To evaluate the anti-inflammatory potential of DCHA, inflammation of the peritoneal tissue of Swiss mice was induced using LPS (500 ng *per* cavity), in which the amount of inflammatory cells that migrated to the peritoneal cavity was observed. The animals were treated with aminoguanidine, naringenin, DCHA, and dexamethasone was used as a standard reference, which is one of the anti-inflammatory steroids of choice for the treatment of chronic inflammatory diseases. All substances were administered orally at a concentration of 1 mg kg^{-1}. In the negative and positive control groups, saline solution (IP) and LPS (IP) were injected, respectively, and both received the vehicle (saline) orally. DCHA effectively reduced leukocyte infiltration in the peritoneal tissue, with no differences between the responses presented by DCHA and dexamethasone (*p* = 0.365), which shows the anti-inflammatory potential of the new carboximidamide (Figure 7). Although the basic structure of DCHA comes
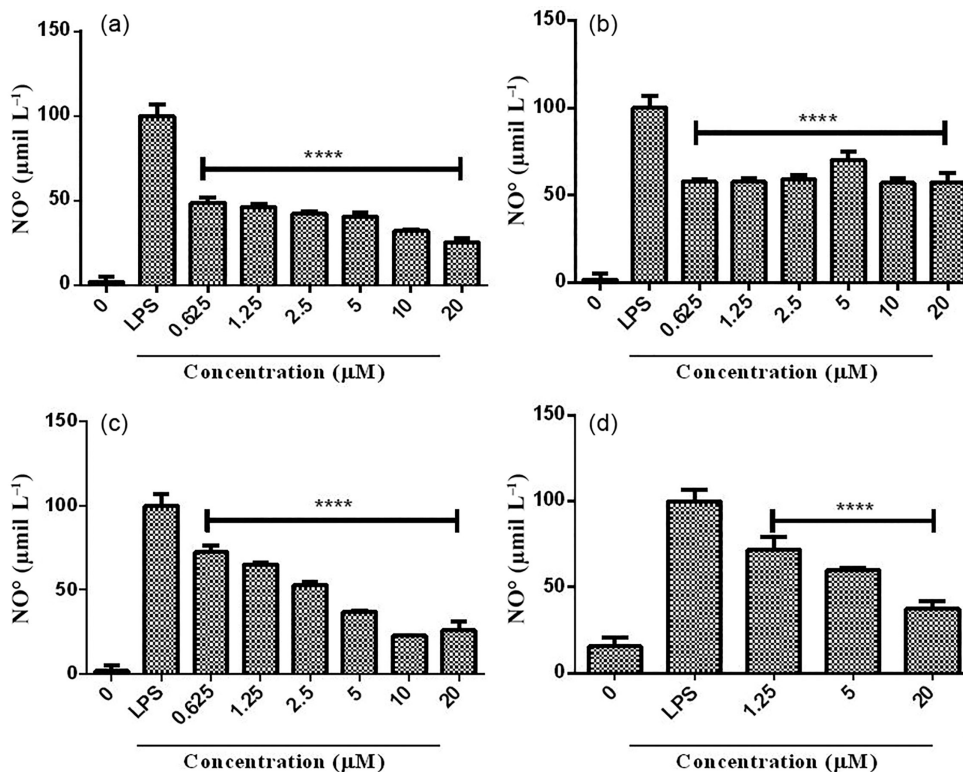
Figure 6. Ability to inhibit the nitric oxide synthesis of DCHA (a), NAR (b), AG (c) and indomethacin (d) in LPS-activated macrophages. Data expressed as mean ± standard deviation, analyzed using two-way ANOVA followed by multiple Newman-Keul comparisons with the LPS group (n = 3, ****$p < 0.0001$).
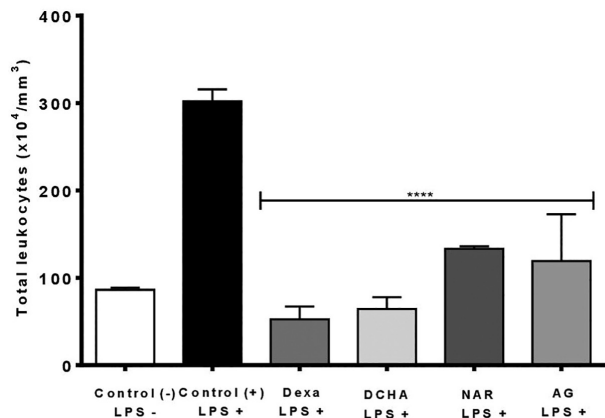

Figure 7. Anti-inflammatory effect and total leukocyte count after 6 h of induction of peritonitis by LPS in mice. Data expressed as mean ± standard deviation, analyzed by two-way ANOVA and followed by multiple Newman-Keul comparisons with the LPS + control group (n = 4, ****$p < 0.0001$). Negative control (CTRL (−) saline); positive control (CTRL (+) saline); dexamethasone (Dexa 1 mg kg^{-1}); DCHA (DCHA 1 mg kg^{-1}); naringenin (NAR 1 mg kg^{-1}); aminoguanidine (AG 1 mg kg^{-1}).

from a flavonoid, this ability to inhibit leukocytes does not come from this chemical entity, since naringenin was shown to be less effective in this inhibition, thus showing that it is a property of the new carboximidamide (DCHA).

It is known that an intraperitoneal injection of LPS triggers the production of cytokines such as IL-1β and TNF-α and also of chemokines, which activate endothelial cells and cause an increase in the expression of adhesion and rolling molecules in leukocytes. These cytokines are important molecules for the recruitment of leukocytes during inflammation and pain caused by LPS.[49] It is hypothesized that the effect of DCHA in inhibiting the local influx of inflammatory leukocytes induced by LPS is in fact by inhibiting the production of inflammatory mediators, and the regulation of these mediators points to a therapeutic potential in the treatment of various inflammatory diseases.

Zymosan-induced paw edema

The DCHA was administered at a concentration of 5 mg kg^{-1} one hour before the induction of edema via plantar inoculation of zymosan. The administered dose of DCHA significantly reduced ($p = 0.00064$) the edema caused by the zymosan. The effect presented by diclofenac ($p = 0.0055$) was significant, however, it was considered that the DCHA administered at a dose of 5 mg kg^{-1} presented a pharmacological response 20 times greater than diclofenac, since this was administered at a dose of 100 mg kg^{-1} (Figure 8). On the other hand, naringenin showed a less significant reduction in the phlogistic reaction of zymosan and aminoguanidine, despite effectively reducing the swelling of the paws of the treated animals; this decrease was smaller than that observed in DCHA. The significant

J. Braz. Chem. Soc. **2024**, *35*, 4, e-20230157

9 of 12

difference (p = value 0.00063) between responses was highlighted in the maximum time of the inflammatory process, which occurred 6 h after induction. The zymosan-induced inflammatory mechanism, which occurs through the activation of toll-like receptors (TLR2 and TLR6) with the stimulation of the nuclear factor kappa-B (NF-KB) pathway, resulted in the production of eicosanoids, NO, inflammatory cytokines (TNF-α, IL-1β, IL-6) and other neutrophil chemotactic agents. Therefore, this leukocyte infiltration contributes to zymosan-induced cytotoxicity.[50]

In a recent study, considerable edema was observed up to 5 h after the intraplantar injection of zymosan in the paw of mice. This was due to the significant recruitment of immune cells, mainly neutrophils (CD45+/Ly6G+) and macrophages (CD45+/Ly6C+/F4 80+). These immunological data, together with edema formation, clearly demonstrated an intense immune response at the site of inflammation.[51]

The anti-inflammatory effect of DCHA was evidenced by the decrease in zymosan-induced paw edema, which is significant in the late phase, and whose main characteristic is the infiltration of leukocytes, thus demonstrating that this effect is associated with the blockade of recruitment of immune cells achieved by carboximidamide.[50]
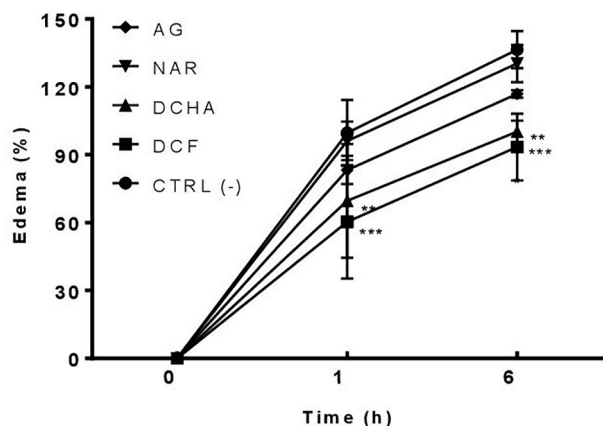

Figure 8. Percentage of paw edema after zymosan induction in mice. Data expressed as mean ± standard deviation, analyzed by two-way ANOVA and followed by multiple Newman-Keul comparisons with the normal group CRTL (−), (n = 4, **$p < 0.00064$; ***$p < 0.0055$). Aminoguanidine (AG 5 mg kg⁻¹); naringenin (NAR 5 mg kg⁻¹); DCHA (DCHA 5 mg kg⁻¹); diclofenac (DCF 100 mg kg⁻¹); negative control (CTRL (−) saline).

Conclusions

For the first time, a condensation reaction between naringenin and aminoguanidine is described, which gave rise to a new flavanone, carboxymidamide (DCHA). This substance inhibited the production of nitric oxide in macrophages stimulated by LPS *in vitro* and *in vivo* inhibited the migration of leukocytes to the peritoneal cavity of mice exposed to LPS, in addition to promoting the reduction of paw edema induced by zymosan. Molecular docking simulations indicated that the anti-inflammatory activity of this new flavanone could be explained by the inhibition of COX-2, iNOS or PDE4 enzymes, with emphasis on the inhibition of iNOS, in which DCHA, *S* and *R* enantiomers, presented higher docking energy than inhibitors, highlighting the *S* enantiomer that interacted more efficiently with the active sites of the tested enzymes. The results obtained show that the new flavanone has the potential to be used in the treatment of inflammatory diseases.

Supplementary Information

Supplementary information (Figures S1-S4) is available free of charge at http://jbcs.sbq.org.br as PDF file.

Author Contributions

R. O. S. S. and E. S. L. were responsible for conceptualization; R. O. S. S. and E. S. L. for methodology; R. O. S. S. and R. A. C. for software; R. O. S. S. and E. S. L. for validation; R. O. S. S. and E. S. L. for formal analysis; R. O. S. S. for investigation; E. S. L. for resources; R. O. S. S. for data curation; L. C. R. H. and A. C. S. P. for writing-original draft preparation; L. C. R. H., A. C. S. P. and R. A. C. for writing-review and editing; visualization, E. S. L.; E. S. L. and F. G. S. for supervision; E. S. L. for project administration; E. S. L. for funding acquisition.

References

1. Sumayya, A. S.; Muraleedhara Kurup, G.; *J. Biomater. Sci., Polym. Ed.* **2021**, *32*, 1040. [Crossref]

2. Serhan, C. N.; Levy, B. D.; *J. Clin. Investig.* **2018**, *128*, 2657. [Crossref]

3. Nunes, C. R.; Arantes, M. B.; Pereira, S. M. F.; da Cruz, L. L.; Passos, M. S.; de Moraes, L. P.; Vieira, I. J. C.; de Oliveira, D. B.; *Molecules* **2020**, *25*, 3726. [Crossref]

4. Cragg, G. M.; Newman, D. J.; *Biochim. Biophys. Acta, Gen. Subj.* **2013**, *1830*, 3670. [Crossref]

5. Cragg, G. M.; Grothaus, P. G.; Newman, D. J.; *J. Nat. Prod.* **2014**, *77*, 703. [Crossref]

10 of 12

J. Braz. Chem. Soc. **2024**, *35*, 4, e-20230157

6. Medina-Franco, J. L.; Saldívar-González, F. I.; *Biomolecules* **2020**, *10*, 1566. [Crossref]

7. Badshah, S. L.; Faisal, S.; Muhammad, A.; Poulson, B. G.; Emwas, A. H.; Jaremko, M.; *Biomed. Pharmacother.* **2021**, *140*, 111596. [Crossref]

8. Yang, O.; Wu, M.; Zhu, Y.-L.; Yang, Y.-Q.; Mei, Y.-Z.; Dai, C.-C.; *Biotechnol. Lett.* **2021**, *43*, 119. [Crossref]

9. Zeng, W.; Jin, L.; Zhang, F.; Zhang, C.; Liang, W.; *Pharm. Res.* **2018**, *135*, 122. [Crossref]

10. Munir, A.; Muhammad, F.; Zaheer, Y.; Ali, A.; Iqbal, M.; Muhammad, M. R.; Munir, U.; Akhtar, B.; Webster, T. J.; Sharif, A.; Ihsan, A.; *J. Drug Delivery Sci. Technol.* **2021**, *66*, 102854. [Crossref]

11. Tutunchi, H.; Naeini, F.; Ostadrahimi, A.; Hosseinzadeh-Attar, M. J.; *Phytother. Res.* **2020**, *34*, 3137. [Crossref]

12. Fan, R.; Pan, T.; Zhu, A. L.; Zhang, M. H.; *Pharmacol. Rep.* **2017**, *69*, 1021. [Crossref]

13. Zhang, S.; Li, D. D.; Zeng, F.; Zhu, Z. H.; Song, P.; Zhao, M.; Duan, J. A.; *Nat. Prod. Res.* **2019**, *33*, 1756. [Crossref]

14. Copmans, D.; Orellana-Paucar, A. M.; Steurs, G.; Zhang, Y.; Ny, A.; Foubert, K.; Exarchou, V.; Siekierska, A.; Kim, Y.; Borggraeve, W.; Dehaen, W.; Pieters, L.; Witte, P. A. M.; *Neurochem. Int.* **2018**, *112*, 124. [Crossref]

15. Joglekar, M. M.; Bavkar, L. N.; Sistla, S.; Arvindekar, A. U.; *Int. J. Biol. Macromol.* **2017**, *99*, 563. [Crossref]

16. Farhad, A. R.; Razavi, S.; Jahadi, S.; Saatchi, M.; *J. Oral Sci.* **2011**, *53*, 225. [Crossref]

17. Misko, T. P.; Moore, W. M.; Kasten, T. P.; Nickols, G. A.; Corbett, J. A.; Tilton, R. G.; McDaniel, M. L.; Williamson, J. R.; Currie, M. G.; *Eur. J. Pharmacol.* **1993**, *233*, 119. [Crossref]

18. Ookawara, M.; Nio, Y.; *Cell. Signal.* **2022**, *90*, 110185. [Crossref]

19. Minhas, R.; Bansal, Y.; Bansal, G.; *Med. Res. Rev.* **2019**, *40*, 823. [Crossref]

20. Fukumoto, S.; Imamya, E.; Kusumoto, K.; Fujiwara, S.; Watanabe, T.; Shiraishi, M.; *J. Med. Chem.* **2002**, *45*, 3009. [Crossref]

21. Trott, O.; Olson, A. J.; *J. Comput. Chem.* **2010**, *31*, 455. [Crossref]

22. Kurumbail, R. G.; Stevens, A. M.; Gierse, J. K.; McDonald, J. J.; Stegeman, R. A.; Pak, J. Y.; Gildehaus, D.; Miyashiro, J. M.; Penning, T. D.; Seibert, K.; Isakson, P. C.; Stallings, W. C.; *Nature* **1996**, *384*, 644. [Crossref]

23. Fedorov, R.; Hartmann, E.; Ghosh, D. K.; Schlichting, I.; *J. Biol. Chem.* **2003**, *278*, 45818. [Crossref]

24. Frisch, M. J.; Trucks, G. W.; Schlegel, H. B.; Scuseria, G. E.; Robb, M. A.; Cheeseman, J. R.; Scalmani, G.; Barone, V.; Petersson, G. A.; Nakatsuji, H.; Li, X.; Caricato, M.; Marenich, A. V.; Bloino, J.; Janesko, B. G.; Gomperts, R.; Mennucci, B.; Hratchian, H. P.; Ortiz, J. V.; Izmaylov, A. F.; Sonnenberg, J. L.; Williams-Young, D.; Ding, F.; Lipparini, F.; Egidi, F.; Goings, J.; Peng, B.; Petrone, A.; Henderson, T.; Ranasinghe, D.; Zakrzewski, V. G.; Gao, J.; Rega, N.; Zheng, G.; Liang, W.; Hada, M.; Ehara, M.; Toyota, K.; Fukuda, R.; Hasegawa, J.; Ishida, M.; Nakajima, T.; Honda, Y.; Kitao, O.; Nakai, H.; Vreven, T.; Throssell, K.; Montgomery, J. A., Jr.; Peralta, J. E.; Ogliaro, F.; Bearpark, M. J.; Heyd, J. J.; Brothers, E. N.; Kudin, K. N.; Staroverov, V. N.; Keith, T. A.; Kobayashi, R.; Normand, J.; Raghavachari, K.; Rendell, A. P.; Burant, J. C.; Iyengar, S. S.; Tomasi, J.; Cossi, M.; Millam, J. M.; Klene, M.; Adamo, C.; Cammi, R.; Ochterski, J. W.; Martin, R. L.; Morokuma, K.; Farkas, O.; Foresman, J. B.; Fox, D. J.; *Gaussian 09*, Revision E.01; Gaussian, Inc., Wallingford, C. T., 2009.

25. Rampersad, S. N.; *Sensors* **2012**, *12*, 12347. [Crossref]

26. Nakayama, G. R.; Caton, M. C.; Nova, M. P.; Parandoosh, Z.; *J. Immunol. Methods* **1997**, *204*, 205. [Crossref]

27. Marques, L. C. F.; Pinheiro, A. J. M. C. R.; Araújo, J. G. G.; Oliveira, R. A. G.; Silva, S. N.; Abreu, I. C.; Sousa, E. M.; Fernandes, E. S.; Luchessi, A. D.; Silbiger, V. N.; Nicolete, R.; Lima-Neto, L. G.; *Planta Med.* **2016**, *82*, 1463. [Crossref]

28. Felix, F. B.; Araújo, J. M. D.; Souza, E. V.; Pinho, V.; Camargo, E. A.; Corrêa, C. B.; Grespan, R.; *Inflamm. Res.* **2020**, *69*, 1245. [Crossref]

29. *GraphPad Prism*, version 6.0.0; GraphPad Software, Boston, USA, 2012.

30. Firouzjaei, F. A.; Heidarli, E.; Ravan, S.; Hosseini, S. M.; Naderi, N.; Almasyan, K.; Sarvary, A.; Irannejad, H.; *Med. Chem. Res.* **2020**, *29*, 1520. [Crossref]

31. Moustafa, A. H.; Ahmed, W. W.; Khodairy, A.; Mabied, A. F.; Moustafa, A.; El-Sayed, M. F.; *J. Mol. Struct.* **2021**, *1230*, 129888. [Crossref]

32. Wei, Z. Y.; Chi, K. Q.; Yu, Z. K.; Liu, H. Y.; Sun, L. P.; Zheng, C. J.; Piao, H. R.; *Bioorg. Med. Chem. Lett.* **2016**, *26*, 5920. [Crossref]

33. Uddin, M. N.; Ahmed, S. S.; Rahatul Alam, S. M.; *J. Coord. Chem.* **2020**, *73*, 3109. [Crossref]

34. Spínola, V.; Llorent-Martínez, E. J.; Gouveia-Figueira, S.; Castilho, P. C.; *Ind. Crops Prod.* **2016**, *90*, 9. [Crossref]

35. Xu, F.; Liu, Y.; Zhang, Z.; Yang, C.; Tian, Y.; *Chin. Med.* **2009**, *4*, 15. [Crossref]

36. Ye, M.; Yang, W. Z.; Liu, K. D.; Qiao, X.; Li, B. J.; Cheng, J.; Feng, J.; Guo, D.-A.; Zhao, Y.-Y.; *J. Pharm. Anal.* **2012**, *2*, 35. [Crossref]

37. Fan, L.-L.; Yi, T.; Xu, F.; Zhang, Y.-Z.; Zhang, J.-Y.; Li, D.-P.; Xie, Y.-J.; Qin, S.-D.; Chen, H.-B.; *Molecules* **2013**, *18*, 15134. [Crossref]

38. de Almeida, M. C. S.; Alves, L. A.; Souza, L. G. S.; Machado, L. L.; de Matos, M. C.; de Oliveira, M. C. F.; Lemos, T. L. G.; Braz-Filho, R.; *Quim. Nova* **2010**, *33*, 1877. [Crossref]

39. Andrade, C. A.; Carvalho, J. L. S.; Cunico, M. M.; Lordello, A. L. L.; Higaskino, C. E. K.; Almeida, S. C. C.; Dias, J. F. G. D.;

J. Braz. Chem. Soc. **2024**, *35,* 4, e-20230157

11 of 12

Kerber, V. A.; Miguel, M. D.; Miguel, O. G.; *Braz. J. Pharm. Sci.* **2010**, *46*, 715. [Crossref]

40. Türkkan, B.; Ozyurek, M.; Bener, M.; Guçlu, K.; Apak, R.; *Spectrochim. Acta, Part A* **2012**, *85*, 235. [Crossref]

41. Celiz, G.; Suarez, S. A.; Arias, A.; Molina, J.; Brondino, C. D.; Doctorovich, F.; *BioMetals* **2019**, *32*, 595. [Crossref]

42. Meng, X. Y.; Zhang, H. X.; Mezei, M.; Cui, M.; *Curr. Comput.-Aided Drug Des.* **2011**, *7*, 146. [Crossref]

43. ISO 10993-5: *Biological Evaluation of Medical Devices - Part 5: Tests for in vitro Cytotoxicity*, ISO: Switzerland, 2009.

44. Park, H. J.; Choi, Y. J.; Lee, J. H.; Nam, M. J.; *Food Chem. Toxicol.* **2017**, *99*, 1. [Crossref]

45. Stompor, M.; Uram, L.; Podg Órski, R.; *Molecules* **2017**, *22*, 1092. [Crossref]

46. Sabuncuoglu, S.; *Mol. Cell. Biochem.* **2014**, *394*, 129. [Crossref]

47. Chao, C. L.; Weng, C. S.; Chang, N. C.; Lin, J. S.; Kao, S. T.; Ho, F. M.; *Nutr. Res.* **2010**, *30*, 858. [Crossref]

48. Heiran, R.; Sepehri, S.; Jarrahpour, A.; Digiorgio, C.; Douafer, H.; Brunel, J. M.; Gholami, A.; Riazimontazer, E.; Turos, E.; *Bioorg. Chem.* **2020**, *102*, 104091. [Crossref]

49. Borghi, S. M.; Mizokami, S. S.; Carvalho, T. T.; Rasquel-Oliveira, F. S.; Ferraz, C. R.; Fattori, V.; Hayashida, T. H.; Peron, J. P. S.; Camilios-Neto, D.; Ambrosio, S. R.; Arakawa, N. S.; Casagrande, R.; Verri Jr., W. A.; *J. Ethnopharmacol.* **2021**, *273*, 113980. [Crossref]

50. Holanda, B. F.; Araujo, D. F.; Silva, J. N. R.; Pereira, M. G.; Pires, A. F.; Assreuy, A. M.; *J. Ethnopharmacol.* **2021**, *267*, 113501. [Crossref]

51. Hahnefeld, L.; Kornstadt, L.; Kratz, D.; Ferreirós, N.; Geisslinger, G.; Pierre, S.; Scholich, K.; *Biochim. Biophys. Acta, Mol. Cell Biol. Lipids* **2021**, *1866*, 158822. [Crossref]